Acta Crystallographica Section D
Biological Crystallography
ISSN 0907-4449

Structure of free fumarase C from *Escherichia coli*

Todd Weaver

Department of Chemistry, University of Wisconsin–La Crosse, 1725 State Street, 4020 Cowley Hall, La Crosse, Wisconsin 54601, USA

Correspondence e-mail: weaver.todd@uwlax.edu

Received 11 March 2005
Accepted 27 July 2005

PDB Reference: fumarase C, 1yfe, r1yfesf.

Previous crystal structures of fumarase C from *Escherichia coli* have noted two occupied dicarboxylate-binding sites termed the active site and the B site. Here, the first known fumarase C structure is reported in which both sites are unoccupied by bound ligand. This so-called 'free' crystal form shows conservation of the active-site water in a similar orientation to that reported in other fumarase C crystal structures. More importantly, a shift of His129 has been observed at the B site. This new crystallographic information suggests the use of water as a permanent member of the active site and the use of an imidazole–imidazolium conversion to control access at the allosteric B site.

1. Introduction

Fumarate hydratase (EC 4.2.1.2), also known as fumarase, catalyzes the reversible hydration/dehydration of fumarate to *S*-malate during the ubiquitous Krebs cycle. Fig. 1 illustrates the fumarase-catalyzed reaction proceeding through the aci-carboxylate intermediate subsequent to olefin production. Members of the fumarase family are identified by the GSS*x*M*x*K*x*N*xx*P*x*E signature sequence (region 3) located between Gly317 and Glu331 [all numbering based upon the fumarase C (FumC) sequence from *Escherichia coli*] and increased homology at two other regions (regions 1 and 2; Fig. 2*a*; Woods *et al.*, 1986). Past FumC structural investigations have noted a dumbbell-shaped monomer structure with three domains (D1, D2 and D3; Fig. 2*a*). Domain 2 consists of a five-helix bundle that forms a 20-superhelix structure upon tetramer formation. Domains 1 and 3 form projections from the D2 core.

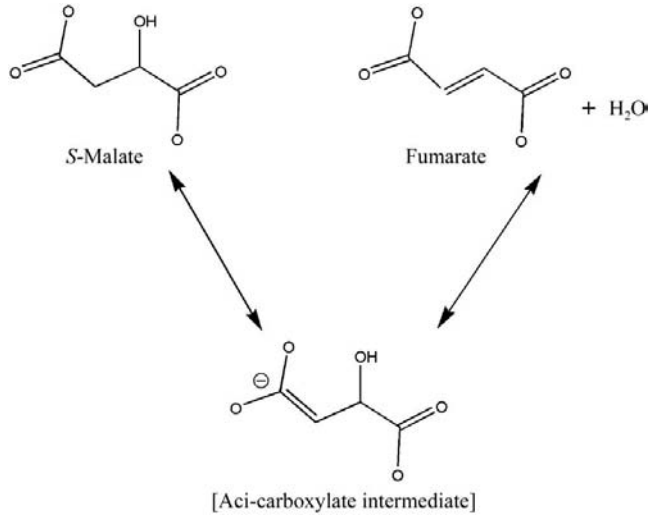

Figure 1
Reaction catalyzed by fumarase.

Previous X-ray crystallographic studies have also reported two dicarboxylate-binding sites located 12 Å from one another (Fig. 2*b*). The first binding site has been identified as the active site and is formed by residues from regions 1–3, where each region is donated by a distinct subunit (Figs. 2*a* and 2*b*). A molecule of citrate and a water molecule were also observed within the active site. The citrate was coordinated in part by both Lys324 and Asn326, while the water molecule (W26) was found to be trapped within the back active-site residues, sharing hydrogen bonds with Ser98, Thr100, Asn141 and His188 (Fig. 2*b*; Weaver & Banaszak, 1996; Weaver *et al.*, 1997).

In contrast to the active site, residues (Arg126–Asn135) involved in the second dicarboxylate site or B site stem from a single subunit donated exclusively from region 1 (Figs. 2*a*, 2*b* and 2*c*). In the 'occupied' FumC crystal structure, a molecule of *S*-malate was shown to be bound to the B site. The carboxylate groups of *S*-malate contact both the Arg126 side-chain atoms and the NH main-chain atoms from Asn131 and Asp132 (Fig. 2*c*; Weaver & Banaszak, 1996). The residues used to construct the B site are derived from the same subunit, which contributes Ser98, Thr100 and Asn141 to the constellation surrounding W26 in the active site. This places the centers of the active and B sites within 12 Å of one another, with the B site closer to the enzyme surface (Fig. 2*b*). An additional crystal structure has also been reported with the *cis* substrate β-trimethylsilylmalic acid bound in place of *S*-malate (Weaver & Banaszak, 1996). This additional crystal structure helped to reaffirm the B site as an extension of the active site as it may provide a route of escape for reaction products.

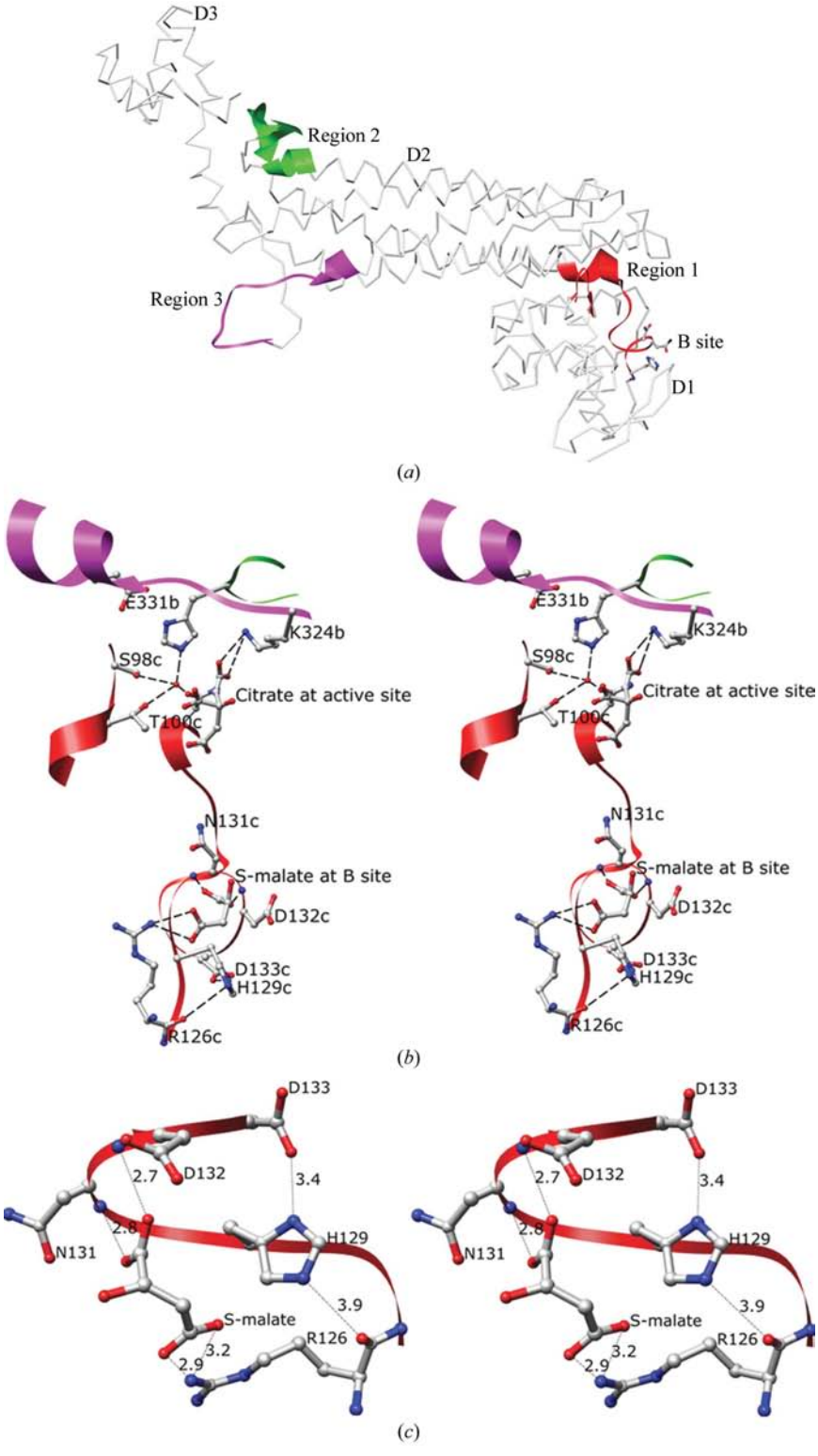

Figure 2
FumC active and B sites. (*a*) A cartoon of the FumC monomer noting the juxtaposition of three highly conserved regions within the superfamily. Region 1 in the *C* subunit (Thr96–Thr100 and His129–Thr146) has been colored red. Region 2 in the *A* subunit (Gly185–Glu200) has been colored green, while region 3 in the *B* subunit (Gly317–Glu331) has been colored magenta. Region 1 also harbors the B site, including His129, Asn131, Asp132, Asp133 and Asn135. Domains 1–3 are labelled D1, D2 and D3, respectively. (*b*) The occupied FumC dicarboxylate-binding sites constructed from regions 1–3 donated by subunits *A*–*C*. The locations of the citrate and W26 approximate the active site, while the location of *S*-malate approximates the B site. The centers of the two dicarboxylate molecules are 12 Å apart. (*c*) Close-up view of *S*-malate binding at the B site in the occupied FumC crystal structure. The binding of *S*-malate is propagated through both side-chain atoms donated from Arg126 and main-chain NH groups donated from Asn131 and Asp132. As a consequence of *S*-malate binding, His129 has rotated out of the B site, where the imidazolium form is stabilized by the carboxylate group of Asp132. All atoms are colored by type: carbon, gray; oxygen, red; nitrogen, blue. The dashed lines represent hydrogen bonds and each residue has a terminal label identifying the contributing subunit. Figs. 2 and 3 were prepared using *Chimera* (Huang *et al.*, 1996) or *O* (Jones *et al.*, 1991).

Past kinetic studies have noted simple anion activation of fumarate to *S*-malate and this was surmised to occur based upon charge replacement during product release (Rose, 1997). In addition, other kinetic investigations have proposed a viscogenic sensitive conformational change as the rate-determining step during the reaction sequence (Rose, 1998). Most recently, kinetic studies have provided evidence that the B site should be considered a functional part of the FumC active site, serving as a stage during the transfer of substrate and product from the bulk solvent to the active site. The negatively charged lining of the FumC active site promotes product release and guidance toward the positively charged B site. Fundamentally, the most recent study reported that the replacement of two basic residues, Arg126 and His129, within the B site greatly decreased product release as the site was concluded to no longer attract the negatively charged *S*-malate molecule (Weaver & Rose, 2004). Unclear from all of these kinetic investigations, however, was a clear mechanism supporting simple anion activation and glycerol-sensitive conformational change.

To date, all FumC structures have reported ligand-occupied active and/or B sites and it remained unclear whether structural rearrangements would occur in an unoccupied or free FumC structure. In addition, the previously reported crystal structures were obtained from crystals grown at pH 6.0 in the presence of the competitive inhibitor citrate (Weaver *et al.*, 1995, 1997; Weaver & Banaszak, 1996). The results reported here describe the first FumC crystal structure in which both the active and B sites are free of bound ligand. This so-called free crystal form grown at pH 7.5 shows preservation of the active-site water, W26, as reported for other occupied FumC crystal structures (Fig. 2*b*). In contrast, the structural results indicate an imidazole–imidazolium-dependent gating at the allosteric B site. The structural results also provide potential mechanisms for simple anion activation and glycerol-sensitive recycling of fumarase after the fumarate→*S*-malate reaction. All comparisons between free FumC, the focus of this study, and occupied FumC utilize the PDB entry 1fuo coordinate file harboring *S*-malate at the B site and citrate at the active site (Fig. 2*b*).

2. Experimental procedures

2.1. Molecular replacement of the free crystal form of FumC

The *I*222 habit reported here as free FumC was crystallized from a solution of 50 m*M* MOPS pH 7.5, 100 m*M* $LiSO_4$ and 12%(*w*/*v*) PEG 4000 (Weaver *et al.*, 1993). X-ray data were collected between 8 and 2.19 Å from a single crystal, resulting in an R_{merge} of 7.0 (Table 1). A single molecule from PDB entry 1fuo was used as a search probe to solve the free FumC crystal structure after removing ligand and water molecules. Cross-rotation functions were calculated with *X-PLOR*, in which the search probe was placed into an orthorhombic box with dimensions a = 180.0, b = 250.0, c = 100.0 Å (Brünger, 1992). The angular search was limited to one asymmetric unit. The cross-rotation function was calculated using X-ray data between 10 and 5.0 Å resolution and $|F(hkl)|$ greater than 2σ. A maximum correlation score for the cross-rotation function was 6.08σ and placed the probe at the angular orientation $\theta_1 = 274.5^\circ$, $\theta_2 = 32.5^\circ$, $\theta_3 = 265.5^\circ$ (Brünger *et al.*, 1998).

Table 1
Refinement statistics for free FumC.

Values in parentheses are for the highest resolution bin (2.27–2.19 Å).

No. of crystals	1
Space group	*I*222
Unit-cell parameters	
a (Å)	121.6
b (Å)	128.0
c (Å)	62.1
Resolution (Å)	8–2.19
Theoretical reflections	24814
Used reflections	21863 (1681)
Test-set reflections	2202 (188)
Data redundancy	2.6 (1.8)
Completeness (%)	98.1 (92.4)
$I/\sigma(I)$	13 (1.4)
Solvent content (%)	50
R_{merge}	7.0 (24.9)
R factor	19.3
R_{free}	20.4
No. of residues	456
Ramanchandran core region (%)	90.8
No. of protein atoms	3464
No. of solvent molecules	112
R.m.s. bond length (Å)	0.006
R.m.s. bond angles (°)	1.24
R.m.s. dihedrals (°)	21.62
Average B factor, side-chain atoms (Å^2)	34.4
Average B factor, main-chain atoms (Å^2)	32.4

The rotated FumC model was then used for the translation solution. A strong solution was found at the fractional coordinates x = 0.008, y = 0.102, z = 0.484. There was one strong peak in the plot prior to PC refinement. After PC refinement, however, there were a number of peaks, but all had almost the same angular orientation. The highest peak was chosen with the angular orientation $\theta_1 = 271.12^\circ$, $\theta_2 = 30.77^\circ$, $\theta_3 = 268.86^\circ$. In the translation search, the highest peak in the rotation function was used along with the free crystal form of FumC with a resolution cutoff between 8.0 and 4.0 Å and $|F(hkl)|$ greater than 2σ. A maximum correlation value of 0.734 with a mean of 0.225 was found at the position x = 0.008, y = 0.102, z = 0.484. The initial R factor was equal to 0.40 for the single subunit within the asymmetric unit (Brünger, 1992). Crystallographic twofold axes were used to generate the biologically relevant tetramer as needed for final model interpretation and drawings.

2.2. Refinement

Prior to the start of refinement, 10% of the structure-factor amplitudes were selected randomly, removed from the refinement and utilized to compute the free R (R_{free}). Rigid-body refinement was used to initiate the refinement scheme. Simulated annealing, including the Powell minimization, was performed within *CNS*, where a residual refinement target was implemented on the all data collected between 8 and 2.19 Å (Brünger *et al.*, 1998). A grouped B-factor refinement procedure was performed following the simulated-annealing and

Powell minimization run. The bulk-solvent correction was omitted owing to a lack of low-resolution data. The data-collection strategy was set to maximize the high-resolution data and therefore the low-resolution data beyond 8 Å were not collected before significant decay was observed in the diffraction pattern. A switch from *X-PLOR* to *CNS* used during the refinement scheme was based upon software availability. After each round of refinement, $2|F_o| - |F_c|$ and $|F_o| - |F_c|$ electron-density maps were computed and the program *O* was used to make model corrections (Jones *et al.*, 1991). In addition, a simulated-annealing omit map was also calculated during the refinement scheme where residues 126–133 were omitted (Fig. 3*a*).

Water molecules obeying proper hydrogen-bonding constraints with electron densities greater than 1σ on a $2|F_o| - |F_c|$ map and 4σ on a $|F_o| - |F_c|$ map were also included as the model neared completion. *PROCHECK* was used on the refined coordinate files to check the stereochemical quality (Laskowski *et al.*, 1993). The resultant Ramanchandran plot displayed 90.8% of residues within the most favored regions. Phe356 was the one residue found within the disallowed region. This residue is positioned between a dimeric interface within the active site directly behind His188 and in this position it seems to fill a non-polar cavity formed by surrounding hydrophobic residues. In essence the disallowed orientation of Phe356 may assist in proper positioning of the active-site groups, including His188. Thr230 was found outside the most favored region but within the generously allowed area of the Ramanchandran plot. Thr230 is also located in close proximity to the three-subunit active site near Asn141 of region 1. Again, the orientation of Thr230 may favor

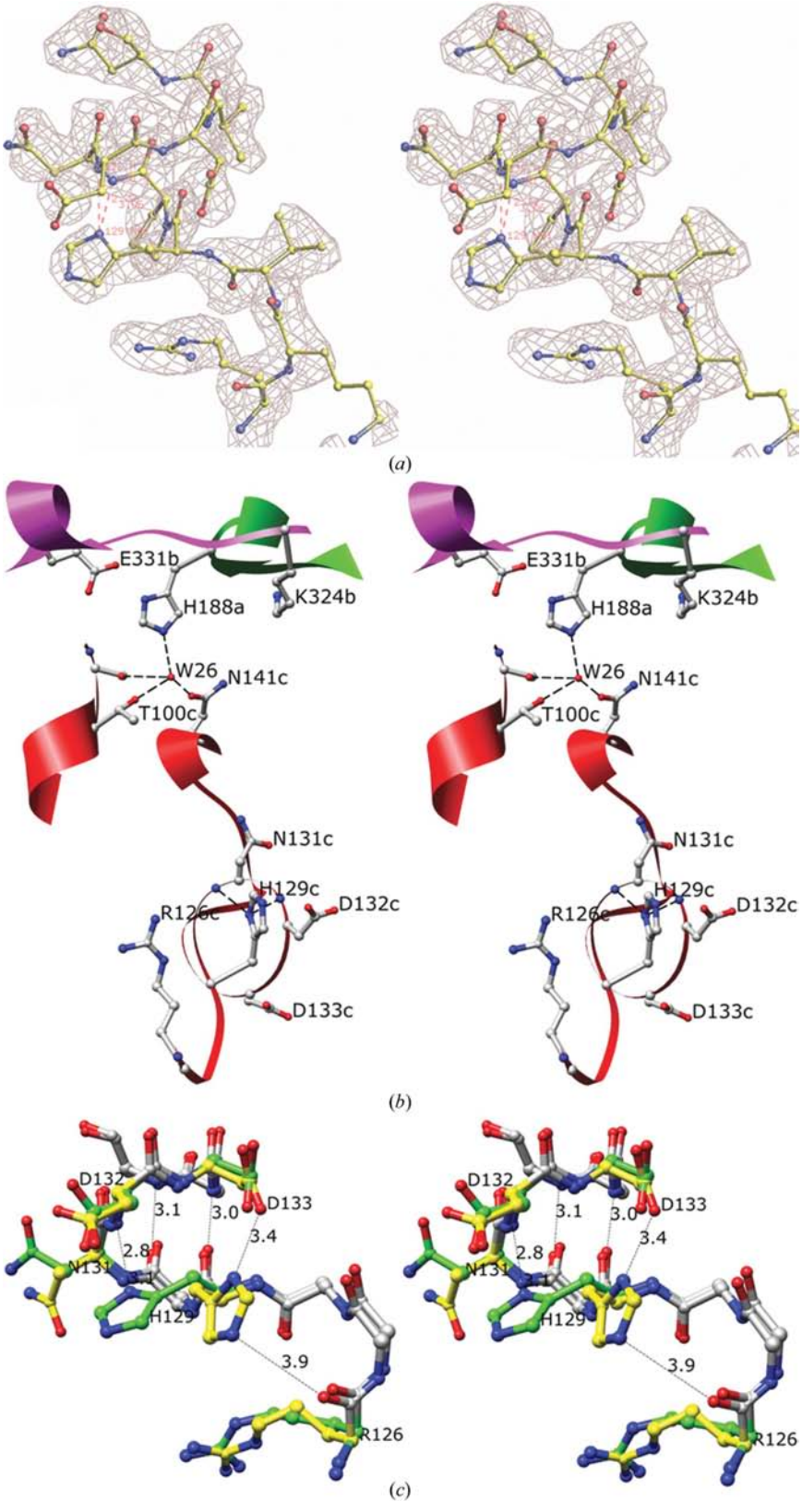

Figure 3
Stereo images of the free FumC crystal structure. (*a*) A representative section of $2|F_o| - |F_c|$ electron density contoured at 1σ from a simulated-annealing omit map where residues 126–133 of the free B site were omitted during the calculation. (*b*) The free FumC active and B sites where His129 has rotated into the B site and forms a bifurcated hydrogen bond with Asn131 NH and Asp132 NH. Color coding and subunit designation is identical to Fig. 2(*b*). (*c*) The free and occupied B sites have been superimposed; C atoms colored green represent the free B site, while those colored yellow represent the occupied B site. In the occupied form, H129 positions itself between Asp133 OD2 and Arg126 O. In the free form, His129 occupies the B site and forms contacts with Asn131 NH and Asp132 NH. Two representative *n*, (*n* + 5) hydrogen bonds within the π-helix region of the B site are represented between His129 O and Val134 NH and between Pro130 O and Asn135 NH as dashed lines. All other atoms are colored by type: carbon, gray; oxygen, red; nitrogen, blue. Dashed lines represent hydrogen bonds or potential sources of stabilizing interactions.

proper positioning of residues intimately involved at the active site, including Asn141. The final structure including protein atoms and solvent molecules was refined to final R factors of 19.3% (R factor) and 20.4% ($R_{\rm free}$). The overall average main-chain B factor was 32.4 Å^2, while the average side-chain B factor was 34.4 Å^2 (Table 1). The symm_obj function within *O* was used to generate the symmetry-related subunits to construct the FumC tetramer for all drawings. The symmetry-transformation matrices have been provided in the header of PDB code 1yfe.

3. Results and discussion

3.1. Active site

Overall, the crystal structure of free FumC shows no large-scale structural differences. Identically to the occupied crystal form, the monomeric structure of free FumC appears to be made up of three domains, with the positions of regions 1–3 far removed from one another (Fig. 2*a*). Past X-ray crystallographic results have shown that residues from three of the four subunits (each donates one of the three regions shown in Fig. 2*a*) within the tetrameric enzyme were used to build each of the four FumC active sites (Weaver *et al.*, 1995). In addition, the occupied FumC active site was shown to use both Asn326 and Lys324 to contact citrate. In the absence of citrate, the free FumC crystal structure shows few movements within the active site. Even Lys324 and Asn326 reveal little shift. The r.m.s.d. for the free and occupied side-chain atoms of Lys324 and Asn326 are 1.3 and 1.6 Å, respectively. The absence of large structural shifts seems plausible unless numerous non-covalent interactions are disrupted simultaneously within the three-subunit interface of the active site.

While there are only slight shifts centered upon Lys324 and Asn326 within the active site, there are even fewer differences between the constellation of atoms surrounding W26 (Fig. 3*b*). The average r.m.s.d. between the free and occupied side-chain atoms of Ser98, Thr100, Asn141 and His188 is 0.25 Å. The stability of the light-atom constellation may provide proper orientation of W26 during its use as a catalytic group within the active site and therefore large structural deviations would not be expected between the free and occupied forms. Past mechanistic arguments have proposed the use of a charge relay between Glu331 and His188 to activate W26 as the active-site nucleophile capable of facilitating abstraction of the C3 proton from *S*-malate (Weaver *et al.*, 1997). The free FumC crystal structure clearly indicates that citrate is not required to maintain W26 within the active site. Rather, it seems that the binding pocket created by Ser98, Thr100, Asn141 and His188 is sufficient to bind W26 (Fig. 3*b*).

3.2. B site

The B site is formed from the same subunit that donates region 1 to the multisubunit FumC active site (Fig. 2*b*). The centers of both binding sites are approximated by the relative position of the bound dicarboxylate molecules and the only access to either site is through an opening near Arg126 on the enzyme surface (Fig. 2*b*). Based upon the approximate centers of citrate and *S*-malate, the two sites are within 12 Å of one another, with the B site nearest the portal to the surrounding external milieu. Beyond the close proximity, the two sites are also connected *via* a series of hydrogen bonds that initiate within Asn131 at the B site and propagate through Ser140 and Asn141 at the active site. Therefore, binding events and movements within the B site could be easily relayed to the active site through this series of interacting hydrogen bonds.

The most significant movements within the free FumC crystal structure are located at the B site, specifically within the side-chain atoms of His129 and Asn131. In occupied FumC reported at pH 6.0, the carboxylate groups of *S*-malate bind to Arg126 side-chain atoms and to NH atoms donated from Asn131 (2.8 Å) and Asp132 (2.7 Å) within the π-helix region (His129–Asn135) of the B site (Figs. 2*b* and 2*c*). At this pH, the imidazolium form of the His129 side chain would be expected. The positive charge on His129 causes it to rotate out of the B site and contact Asp133 OD2 (3.4 Å) and Arg126 O (3.9 Å) (Fig. 3*c*). In the free form reported here at pH 7.5, the His129 side chain would be expected to exist primarily in the unprotonated imidazole form. In the imidazole form, a χ_1/χ_2 rotation within the side chain of His129 repositions the ND1 atom within 2.8 and 3 Å of Asp132 NH and Asn131 NH, thereby blocking the B site (Figs. 3*b* and 3*c*). An additional consequence of the movement of His129 into the B site results in a shift of the Asn131 side chain (90° about χ_1) toward the active site (Figs. 3*b* and 3*c*). The rotation of His129 in free FumC is similar to the movement observed within the H129N B-site mutant. In the H129N crystal structure, the carboxyamide group from Asn129 swung into the B site and replaced *S*-malate by forming a bifurcated hydrogen bond with Asn131 NH and Asp132 NH. In this orientation, the carboxyamide group of Asn129 maintained hydrogen bonds within the π-helix region of the B site. While the H129N mutation created a significant shift within the B site, this movement was shown not to perturb citrate binding at the active site, which is similar to the results for the free FumC crystal structure (Weaver *et al.*, 1997). Ultimately, the replacement of the pH-sensitive imidazole ring with the pH-insensitive carboxyamide moiety was accommodated by rotations about χ_1 and χ_2 (Weaver *et al.*, 1997).

It should be emphasized that the same purified pool of FumC was used to generate both the occupied and free crystal forms. The only major difference between the occupied and free crystallization conditions arises from the pH. The occupied form crystallizes at pH 6.0, while the free form crystallizes at pH 7.5. It is also important to note that *S*-malate was never added to the either crystallization condition and its presence within the occupied FumC crystal structure has been attributed to the affinity purification scheme that was used. Thus, *S*-malate was present at identical concentrations during crystallization of both the free and occupied forms and the differences observed at the B site seem to be pH-dependent.

Movements of His129 may provide one or more of three functions: (i) blocking the binding of non-specific dicarboxylate compounds to the positively charged and

surface-exposed B site, (ii) stabilizing the π-helix within the B site and (iii) enhancing product release. Role (i) seems obvious in that blocking the unoccupied B site *via* χ_1/χ_2 rotations of His129 provides assurance that other appropriately sized dicarboxylate molecules would not compete with fumarate or *S*-malate for the active site, which is located 12 Å away (Fig. 3*b*).

Role (ii) would assure the integrity of the B site in the absence of bound dicarboxylate. In the occupied FumC crystal structure, one of the carboxylate groups of *S*-malate contacts the NH main-chain atoms of Asn131 and Asp132. A shift of His129 about χ_1/χ_2 places the unpaired electrons of His129 ND1 within 3 and 2.8 Å of Asn131 NH and Asp132 NH, respectively, and in the absence of dicarboxylate this may stabilize the n, $(n + 5)$ hydrogen-bonding network within this π-helix region (Fig. 3*c*). To date, it is not known whether perturbation of the B-site conformation will affect the active-site conformation. However, it does seem plausible that movements within the B site would propagate to the active site, as residues from the same subunit construct both sites (Fig. 3*b*).

Role (iii) stems from the reversible protonation/deprotonation of His129 when shifting between the two crystallization conditions (free, pH 7.5 and occupied, pH 6.0). The imidazole (free) to imidazolium (occupied) conversion would cause disruption of the bifurcated hydrogen bond noted between His129 ND1, Asn131 NH and Asp132 NH (Fig. 3*c*). The pH-sensitive gating at the B site may help describe both the glycerol-sensitive conformational change that has been described for fumarase and the k_{cat}/K_m enhancements observed in the presence of simple anions at pH values of $\sim$6.5. In the absence of anions, glycerol was shown to decrease both the V_{max} and V_{max}/K_m values, which indicated that the glycerol-sensitive step occurred either before or coincidentally with *S*-malate release. Based upon the free FumC crystal structure, this glycerol-sensitive step could be attributed to the movement of the imidazole ring from His129 through the viscous medium and into the B site (Figs. 3*b* and 3*c*).

The simple anion-dependent k_{cat}/K_m enhancement within fumarase has been attributed to a simple electrostatic effect. In the proposed scheme, simple anions neutralize positive charges on the enzyme surface, which then prevents recapture of the negatively charged product and enhances release (Rose, 1998). Again based upon the free FumC crystal structure, the B site would harbor the positive charges (Arg126, Lys127 and His129) neutralized by the simple anions. In addition, simple anion rate enhancement was maximal at pH $\simeq$ 6.5 and diminished above pH 8.0. This statement can also be supported by comparison of the free (pH 7.5) and occupied (6.0) FumC models. At pH 6.5 or below, His129 exists in the imidazolium state and presumably flips out of the B site, thereby leaving access to dicarboxylate molecules and simple anions (Fig. 2*c*). Binding of simple anions to the B site would then neutralize its positive charge and facilitate product release. At pH 8.0 or above, which is similar to the pH of the buffer system used to grow the free FumC crystal form, the anion effect diminishes. Based upon the free FumC crystal structure, this would be attributed to deprotonation of the imidazolium form of His129 at pH 7.5 and subsequent rotation into the B site to form a bifurcated hydrogen bond to Asn131 NH and Asp132 NH (Fig. 3*c*). This movement effectively blocks access to the B site to small anions, thereby preventing potential activation.

4. Summary

There are a number of other enzymes and at least one ion channel that have been shown to utilize reversible protonation/deprotonation to transport protons (Adelroth *et al.*, 2001; Admiraal *et al.*, 1999; Hopkins *et al.*, 2002; Huang & Tu, 1997; Lehoux & Mitra, 1999; Matsunami *et al.*, 2004; Tu *et al.*, 2002; Venkataraman *et al.*, 2005). Furthermore, in one enzyme instance the reversible protonation states have been linked to histidine side-chain movements (Fisher *et al.*, 2005). In the case of human carbonic anhydrase II, the crystal structures reported at pH 8.5 and 5.7 were very similar except for the conformation of His64, the catalytic proton-shuttle residue (Nair & Christianson, 1991). The side chain of His64 was reported to rotate away from the active site by 64° about χ_1 in the pH 5.7 crystal form. The movement of His64 in and out of the active site was proposed to be consistent with the reversible hydration/dehydration reaction catalyzed by carbonic anhydrase. During the hydration reaction, the inward-facing imidazole form of His64 accepts a proton from the zinc-bound water molecule, rotates abut χ_1 and thus converts to the outward-facing imidazolium form to deliver the proton to the solvent (Fisher *et al.*, 2005).

Copper amine oxidase is another enzyme where histidine side-chain movements have been observed in crystal structures. Copper amine oxidase requires TOPA-quinone (TPQ) to catalyze the oxidation of primary amines. The organic cofactor TPQ is produced *via* an autocatalytic copper-dependent post-translational oxidative modification of an existing tyrosine residue within copper amine oxidase. Two distinct conformers of His592 have been noted within copper amine oxidase and differ by 70° about χ_1 (Matsunami *et al.*, 2004). These movements are afforded owing to the presence of a large area beside the imidazole ring. The exact function of His592 side-chain movements are not known, but it is believed that its coordination to the Cu atom optimizes the active site during the oxidation of primary amines (Matsunami *et al.*, 2004).

For FumC, the reversible protonation/deprotonation of His129 seems most similar to that observed within human carbonic anhydrase II, as the χ_1 conformational change seems driven by a pH-dependent imidazole (pH 6.0, occupied) to imidazolium (pH 7.5, free) conversion. In the human carbonic anhydrase instance, this pH-dependent conversion allows His64 to rotate in and out of the active site as protons shuttle during the catalytic cycle. For FumC, the imidazole to imidazolium conversion controls access at the B site, which is only 12 Å away from the active site (Figs. 2*b* and 3*b*). Gating of this nature could help describe the activation of fumarase by simple anions. In the open state, a simple anion may bind and

occupy the positively charged B site. This may facilitate release of products in two fashions: (i) by preventing access to the positively charged B site as negatively charged products are formed within the active site and (ii) by providing an electrostatic repulsive force as products move out of the back of the active site, past the B site and into the surrounding solvent.

The author is grateful to Ed Hoeffner for his contributions to this study through the maintenance of the X-ray facilities at the University of Minnesota. TW acknowledges Dean Michael Nelson and the Dean's Summer Fellowship Program within the College of Science and Allied Health at the University of Wisconsin–La Crosse for their continued support of undergraduate research. The research was supported through both a Cottrell College Science Award (CC6064) from Research Corporation and a University of Wisconsin–La Crosse Faculty Research Award to TW.

References

Adelroth, P., Paddock, M. L., Tehrani, A., Beatty, J. T., Feher, G. & Okamura, M. Y. (2001). *Biochemistry*, **40**, 14538–14546.

Admiraal, S. J., Schneider, B., Meyer, P., Janin, J., Veron, M., Deville-Bonne, D. & Herschlag, D. (1999). *Biochemistry*, **38**, 4701–4711.

Brünger, A. T. (1992). *X-PLOR Version 3.1. A System for X-ray Crystallography and NMR.* Yale University, Connecticut, USA.

Brünger, A. T., Adams, P. D., Clore, G. M., DeLano, W. L., Gros, P., Grosse-Kunstleve, R. W., Jiang, J.-S., Kuszewski, J., Nilges, N., Pannu, N. S., Read, R.J., Rice, L. M., Simonson, T. & Warren, G. L. (1998). *Acta Cryst.* D**54**, 905–921.

Fisher, Z., Hernandez Prada, J. A., Tu, C., Duda, D., Yoshioka, C., An, H., Govindasamy, L., Silverman, D. N. & McKenna, R. (2005). *Biochemistry*, **44**, 1097–1105.

Hopkins, C. E., O'Connor, P. B., Allen, K. N., Costello, C. E. & Tolan, D. R. (2002). *Protein Sci.* **1**, 1591–1599.

Huang, C. C., Couch, G. S., Pettersen, E. F. & Ferrin, T. E. (1996). *Pac. Symp. Biocomput.* **1**, 724.

Huang, S. & Tu, S.-C. (1997). *Biochemistry*, **36**, 14609–14615.

Jones, T. A., Zou, J. Y., Cowan, S. W. & Kjeldgaard, M. (1991). *Acta Cryst.* A**47**, 110–119.

Laskowski, R. A., MacArthur, M. W., Moss, D. S. & Thornton, J. M. (1993). *J. Appl. Cryst.* **26**, 283–291.

Lehoux, I. E. & Mitra, B. (1999). *Biochemistry*, **38**, 9948–9955.

Matsunami, H., Okajima, T., Hirota, S., Yamaguchi, H., Hori, H., Kuroda, S. & Tanizawa, K. (2004). *Biochemistry*, **43**, 2178–2187.

Nair, S. K. & Christianson, D. W. (1991). *Biochem. Biophys. Res. Commun.* **181**, 579–584.

Rose, I. A. (1997). *Biochemistry*, **36**, 12346–12354.

Rose, I. A. (1998). *Biochemistry*, **37**, 17651–17658.

Tu, C., Rowlett, R. S., Tripp, B. C., Ferry, J. G. & Silverman, D. N. (2002). *Biochemistry*, **41**, 15429–15435.

Venkataraman, P., Lamb, R. A. & Pinto, L. H. (2005). *J. Biol. Chem.* **280**, 21463–21472.

Weaver, T. M. & Banaszak, L. J. (1996). *Biochemistry*, **35**, 13955–13965.

Weaver, T. M., Lees, M. & Banaszak, L. J. (1997). *Protein Sci.* **6**, 834–842.

Weaver, T. M., Levitt, D. G. & Banaszak, L. J. (1993). *J. Mol. Biol.* **231**, 141–144.

Weaver, T. M., Levitt, D. G., Donnelly, M. I., Wilkens-Stevens, P. P. & Banaszak, L. J. (1995). *Nature Struct. Biol.* **2**, 654–662.

Weaver, T. M. & Rose, I. A. (2004). *Proc. Natl Acad. Sci. USA*, **101**, 3393–3397.

Woods, S. A., Miles, J. S., Roberts, R. E. & Guest, J. R. (1986). *Biochem. J.* **237**, 547–557.